Spectroscopic mapping polarimetry in Bragg Micro-cavities

Author: David Ramos Santesmases
Advisor: Oriol Arteaga
Facultat de Física, Universitat de Barcelona, Diagonal 645, 08028 Barcelona, Spain.*

Abstract: We implement a method to spectroscopically map the Mueller matrix of a sample. This measurement is made on a Mueller matrix polarimeter that uses 4 photoelastic modulators and motorized sample positioners. This technique is applied to the study of the anisotropic optical properties of multilayer samples consisting of Bragg micro-cavities fabricated via Oblique Angle Deposition.

I. INTRODUCTION

The Mueller matrix is a useful mathematical tool to characterize the optical properties of a medium at certain wavelength. A wide range of polarization-depending optical properties of the material can be calculated from an experimentally measured Mueller matrix. Using a Mueller matrix polarimeter with four photoelastic modulators (PEMs) introduced in [1] all the elements of the Mueller matrix can be simultaneously determined.

A common trend associated with the progress of nanotechnology is the need for studying increasingly complex structures in which the optical effects are not homogeneous across the sample and their spatial dependence has to be measured.

The use of a microscope that could measure simultaneously all the Mueller matrix elements with high spatial resolution [2] was discarded as the optical properties of the samples considered in this work vary over a large area. The approach followed in this work has been to automatize a procedure to map the samples point by point. With the data obtained an image representing a space-resolved measurement of the Mueller matrix has been generated.

Our technique will be tested on samples consisting of Bragg micro-cavities fabricated via Oblique Angle Deposition (OAD) [3] and supplied by researchers at the Instituto de Ciencia de Materiales de Sevilla (ICMS).

OAD constitutes a straightforward method to fabricate nanostructured columnar architectures. One of the possibilities of this technique is the control of the refractive index of the films by tuning their porosity. Optical properties of OAD thin films are closely related not only to their composition but also their microstructure. Thus, even if at atomic scale the constituent material is isotropic, asymmetric columnar structure and lateral connectivity of nanocolumns may contribute to induce the development of an anisotropic optical response.

In addition to the spatially resolved information, the accurate study of Bragg micro-cavities requires the spectral dependence of the optical properties. The main drawback of making this kind of studies is the amount of time required to perform both types of analysis (spectrally and spatially resolved). The objective of this work is to implement spectroscopic mapping software in the 4-PEM Mueller matrix polarimeter to automatize these measurements.

II. THEORY AND ISTRUMENTATION

A. Mathematical description

The most convenient way to describe the polarization effects of the optical elements in the 4-PEM polarimeter and the polarization-changing sample is the Stokes–Mueller calculus. This formalism describes the state of polarization by means of the Stokes vector, given by:

$$\boldsymbol{S} = \begin{pmatrix} I \\ Q \\ U \\ V \end{pmatrix} = \begin{pmatrix} \langle |E_x|^2 + |E_y|^2 \rangle \\ \langle |E_x|^2 - |E_y|^2 \rangle \\ \langle E_x^* E_y + E_x E_y^* \rangle \\ i\langle E_x^* E_y + E_x E_y^* \rangle \end{pmatrix}, \qquad (1)$$

where I, Q, U and V are the Stokes parameters, and E_x, E_y the amplitudes of the electric field.

The change of the state of polarization of a light beam resulting from its interaction with an optical element (via transmission, reflection, or scattering) is represented by the transformation matrix:

$$\mathbf{S_{OUT}} = \mathbf{M}\mathbf{S_{IN}}, \qquad (2)$$

where the Mueller matrix, $\boldsymbol{M}$, is a 4x4 real matrix which represents the polarization-altering properties of the object. A normalized $\boldsymbol{M}$ can be presented as:

$$\bar{\boldsymbol{M}} = \begin{pmatrix} 1 & m_{01}/m_{00} & m_{02}/m_{00} & m_{03}/m_{00} \\ m_{10}/m_{00} & m_{11}/m_{00} & m_{12}/m_{00} & m_{13}/m_{00} \\ m_{20}/m_{00} & m_{21}/m_{00} & m_{22}/m_{00} & m_{23}/m_{00} \\ m_{30}/m_{00} & m_{31}/m_{00} & m_{32}/m_{00} & m_{33}/m_{00} \end{pmatrix}, \qquad (3)$$

where m_{00} is a gain for unpolarised incident light and it must hold the inequality $m_{00} > 0$. The normalized Mueller matrix (3) is obtained by scaling the matrix to m_{00}. The elements of a normalized Mueller matrix have values between -1 and 1. All the experimental Mueller matrices that will be shown in this work are normalized.

The polarization effects that will be relevant for this work, are described in Table 1 in terms of the optical constants (refractive index, n, and absorption coefficient, k, along different directions). To obtain them from the Mueller Matrix, decomposition or an analytic inversion from the experimental Mueller matrix to a Jones matrix is needed. This calculus is explained in [4].

* Electronic address: dramossa12@alumnes.ub.edu

Effect	Symbol	Definition
Horizontal linear dichroism projection	LD	$\frac{2\pi}{\lambda}(k_x - k_y)l$
Horizontal linear birefringence projection	LB	$\frac{2\pi}{\lambda}(n_x - n_y)l$
45º linear dichroism projection	LD'	$\frac{2\pi}{\lambda}(k_{45} - k_{135})l$
45º linear birefringence projection	LB'	$\frac{2\pi}{\lambda}(k_{45} - k_{135})l$

TABLE I: Description of the studied optical parameters. *Subindices of the refractive index and absorption coefficient refer to the directions of the laboratory reference system. This means that if the sample is rotated, these coefficients will change.

The information provided by the parameters LD and LD' can be alternatively expressed in terms of the magnitude and its orientation with respect to the horizontal (x) laboratory axis using the following relations from [4]:

$$LD \text{ magnitude} \propto \sqrt{LD^2 + LD'^2} \quad (4)$$

$$LD \text{ orientation} = \frac{1}{2}\arctan\frac{LD'}{LD} \quad (5)$$

Definitions for LB magnitude and LB orientation are analogous. These four parameters are the ones that will be presented in the spectral evolution.

The arctangent function used in the software is $\arctan2(x,y)$ a function of two arguments in order to return the angle in the appropriate quadrant.

B. Device. Working principle

The Mueller Matrix polarimeter that we have used is based on PEMs. A PEM is an optical device used to alter the polarization of light. The principle of operation of photoelastic modulators is based on the photoelastic effect. A current through a piezoelectric transducer makes the optical element vibrate at its resonant frequency, the consequent stretch and compression involves changes in birefringence. This resonant character allows large amplitude modulation, but also for the same reason, the operation of a PEM is limited to a single frequency (around 50 kHz).The 4-PEM polarimeter works in transmittance and from the analysis of the frequencies of the time-dependent intensity of the light after the polarization state analyser all the Mueller matrix coefficients are determined. The polarization state generator (PSG) and the polarization state analyser (PSA) are composed of a polarizer and two PEMs. The Mueller matrices of a polarizer and a modulator are $\boldsymbol{M_p}$ and $\boldsymbol{M_m}$ respectively [1].

$$\boldsymbol{M_p} = \begin{pmatrix} 1 & 1 & 0 & 0 \\ 1 & 1 & 0 & 0 \\ 0 & 0 & 0 & 0 \\ 0 & 0 & 0 & 0 \end{pmatrix}, \boldsymbol{M_m} = \begin{pmatrix} 1 & 0 & 0 & 0 \\ 0 & 1 & 0 & 0 \\ 0 & 0 & Y_\delta & X_\delta \\ 0 & 0 & -X_\delta & Y_\delta \end{pmatrix} \quad (6)$$

Where $Y_\delta \equiv \cos(\delta)$ and $X_\delta \equiv \sin(\delta)$ and δ is the time dependant retardation introduced by the PEM:

$$\delta = A\sin(\omega t + \varphi) \quad (7)$$

With A representing the amplitude of modulation, ω the frequency of the modulator, and φ the phase. Considering that the input light is unpolarised, and that the azimuthal angles of the first polarizer (P0), the first PEM (PEM0) and the second PEM (PEM 1) are, respectively, θ_{p0}, θ_{m0}, and θ_{m1}. The stokes vector for the PSG is:

$$\boldsymbol{S_{PSG}} = \frac{I_0}{2}\boldsymbol{R}(-\theta_{m1})\boldsymbol{M_{m1}}\boldsymbol{R}(\theta_{m1})\boldsymbol{R}(-\theta_{m0})\boldsymbol{M_{m0}} \text{ x } \boldsymbol{R}(\theta_{m0})\boldsymbol{R}(-\theta_{p0})\boldsymbol{M_{p0}}\boldsymbol{R}(\theta_{p0})(1\ 0\ 0\ 0)^T \quad (8)$$

An analogous calculation can be made for the PSA considering that the light first passes through the third and fourth PEM and finally through the second polarizer.

$$\boldsymbol{S_{PSA}}^T = (1\ 0\ 0\ 0)\boldsymbol{R}(-\theta_{p1})\boldsymbol{M_{p1}}\boldsymbol{R}(\theta_{p1}) \text{ x } \boldsymbol{R}(-\theta_{m3})\boldsymbol{M_{m3}}\boldsymbol{R}(\theta_{m3})\boldsymbol{R}(-\theta_{m2})\boldsymbol{M_{m2}}\boldsymbol{R}(\theta_{m2}), \quad (9)$$

with the rotation matrix $\boldsymbol{R}(\alpha)$ defined in [5].

The intensity of the outgoing beam is then given by:

$$I(t) = \boldsymbol{S_{PSA}^T M S_{PSG}} \quad (10)$$

This last equation shows that the Mueller matrix of the sample can be obtained with the intensity over the time and δ over the time of each PEM, which are the known variables of the problem.

The sample is mounted in a sample holder paced on a platform. This mechanism can be moved by 2 independent motors in order to control the displacement in X and Y respectively. The use of these motors allow us to take measurements in multiple positions of the samples and generate the maps. The 4-PEM also includes a monochromator after the $\boldsymbol{S_{PSA}}$ driven by another motor to control the wavelength to analyse.

III. SAMPLE DESCRIPTION

A. Deposition Method

The analysed sample was obtained through OAD. One of the most remarkable features of this technique is the control the three-dimensional growth achievable with macro-rotation movements of the sample. The main mechanism controlling the nanostructural evolution of the films is a "shadowing effect" that prevents the deposition of particles behind the initially formed nuclei.

Fig. (1), obtained from [3], presents a scheme of the OAD geometrical configuration during deposition from an e-beam evaporation source. The scheme (Fig. (1a)) describes the geometrical parameters relevant to the OAD growth, namely the zenithal angle of alignment between the source and the film (α), the azimuthal angle (ϕ) and the polar angles (δ) and (θ).

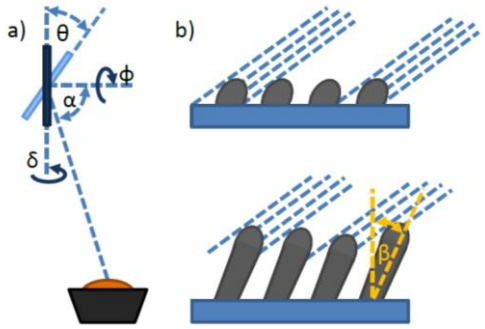

FIG. 1: OAD deposition process. a) Definition of deposition angles. b) Scheme showing the effect of shadowing during the initial and subsequent stages.

Fig. (1 b) illustrates the most basic notions of OAD of thin film showing that the first nuclei formed during the earliest stages of deposition project a shadow behind them that prevents the deposition of any further evaporated material within the "shadowed" areas. As the deposition progresses, these nuclei induce the formation of tilted and separated nanocolumns.

Optical properties of OAD thin films are closely related not only to their composition but also their microstructure. One of the possibilities offered by this technique is the tunability of the refractive index of the films by tuning their porosity/density which can be controlled by the deposition angle α.

B. Bragg Micro-cavities

The studied Bragg micro-cavities are made of alternated layers of TiO_2 and SiO_2 deposited by OAD. Each sample consisting of 2x7 individual layers of approximately 85 nm thickness, plus one SiO_2 middle layer of approximately 180 nm thickness. The porous layers were successively evaporated on glass plates at a zenithal angle $\alpha=80^o$ during a continuous azimuthal rotation process. The fabrication process led to columnar arrangements with inclination angles β (Fig.(1)) depending on the distance from the centre, being 0 at the centre and maximum at the edges. The direction of inclination is always radial with respect to the centre. This process also produced a difference in thickness among the sample, with thicker films at the centre.

The large contrast between the refractive index of the individual SiO_2 and TiO_2 layers of the OAD micro-cavities give rise to interesting optical properties (Fig. (2)). Note that despite the layers of TiO_2 and SiO_2 are transparent in the visible range, the periodic variations of the refractive index creates a complicated spectral response, as it will be discussed later.

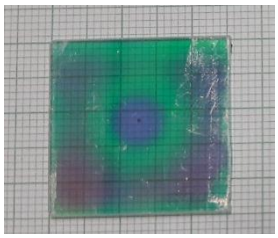

FIG. 2: Image of the studied Bragg Micro-cavity deposited on glass (2.5x2.5 cm^2).

IV. MESUREMENTS

A. Software implementation

The main objective of this work was to obtain the spectral evolution of the Mueller matrix at every point of the sample. To achieve this goal modifications in two parts of the software (LabVIEW based) of the 4-PEM polarimeter were made. The first one is referred to the operation and data acquisition and the other one is for the data visualization. Both programs had to be improved in order to add the spectral mapping option.

In the previous version of the 4-PEMs software the options of mapping and spectral response were already implemented, but only at a certain wavelength or at a certain point of the sample respectively. The results were displayed as spectral responses for each $\mathbf{m_{ij}}$ or in 4x4 images, with each pixel displaying the corresponding value of $\mathbf{m_{ij}}$ at a particular wavelength.

The first step was to automatize the acquisition process of the spectral mapping, to do so, the program had to acquire a mapping response of the Mueller matrix, save it to a text file labelled with a tag of the wavelength used, and once finished should rotate the grating of the monochromator in order to change the wavelength. This step had to be looped over all the desired wavelengths. The inputs of this option are: initial wavelength, final wavelength, step between wavelengths, and name of the document to save the data. The output is a text file with the mapping data for each wavelength, all the text files with the same name except from the label of the wavelength.

The easiest way to visualize the measured data is a video. The structure of the data visualization program is the same as the one used in the acquisition, but now the loop goes through all the text files. In the front panel of LabVIEW we display the Mueller matrix maps which are constantly refreshed for each wavelength. Inputs: name of the file without the wavelength tag, initial wavelength and final wavelength (with no need of being the same that the acquired ones, this allows to take a full spectral acquisition and then focus on the most relevant part of the spectrum), frames per second and number of cycles. The output was the spectral evolution of the Mueller matrix elements, in form of temporal evolution. This software improvement was made extensive to the physical parameters of Table 1 in order to show their spectral evolution in a continuous way.

B. Sample analysis

A preliminary analysis of the spectral response pf the micro-cavity structure has been made by transmission spectroscopy. Fig. (3) shows the measured spectra obtained at different points along a line that crosses the centre of the micro-cavity.

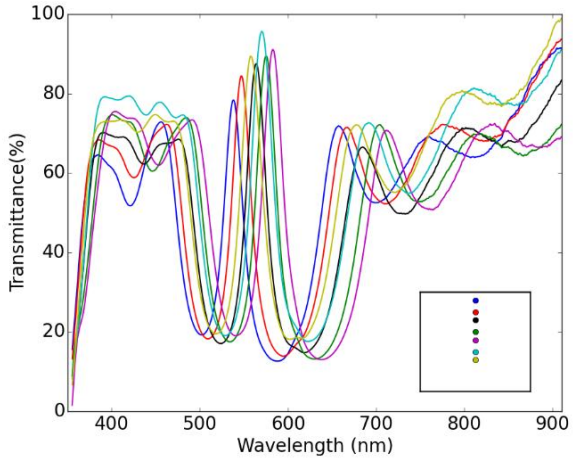

FIG. 3: Transmittance response at different points of the Bragg micro-cavity. The bottom right square represents the sample and the coloured dots stand for the studied positions in the transmittance experiment.

This spectrum depicts the typical behaviour of a Bragg reflector where the alternation of high and low index layers crates a high reflection window (in our case 500 to 650 nm). Delimiting the defect with two high reflection stacks a resonant cavity scheme is introduced. This structure enhances a narrow and sharp transmission maximum (Bragg peak) in the reflective region.

As pointed in section III.B layers' thickness is not homogenous all over the sample. In Figure 2 this phenomena can be appreciated as the peak of transmittance is shifted as we move from the center in a radial direction. On the other hand, the fact that deposition process led to a symmetric deposition can also be appreciated in the spectral response, as the peak displacement is equal at the two sides of the central point (magenta) of the studied line.

The measurements with the 4-PEM polarimeter were made within a centred region of 16x16 mm^2, sampled in steps of 0.5 mm which entails 1024 measurements for each m_{ij}. Each matrix had to be obtained at a wavelength. The spectral evolution ranged from 500nm to 578nm in 2nm steps. A frame of the resulting Mueller matrix spectral evolution in Fig. (4).

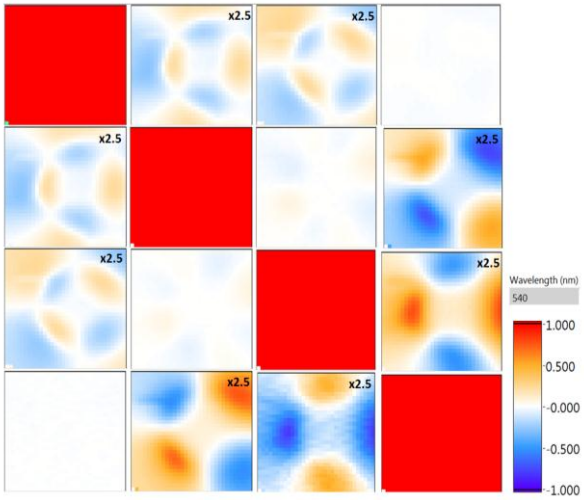

FIG. 4: Mapping of the sample shown in Fig. (2) measured at 540 nm.

With the implemented application the setting was ready in 5-10 minutes to take more than 10 hours of measurements without human intervention.

The physical information usually cannot be directly visualized in the Mueller matrix. It is better to present the results in terms of the physical parameters of Table 1. In Fig. (5) we display the spectral evolution of those properties for a point in the sample.

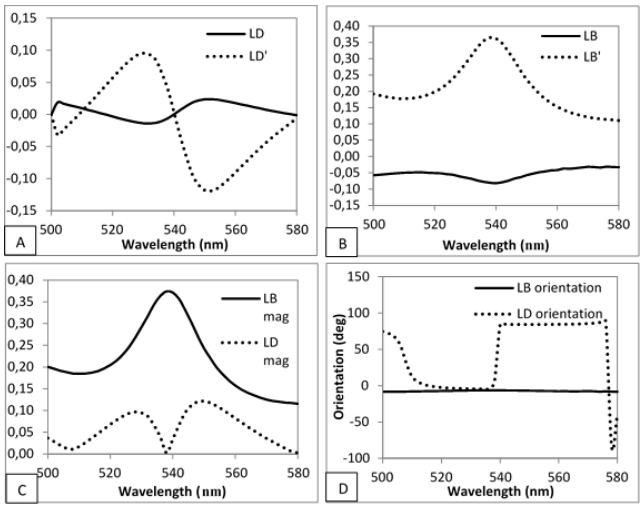

FIG. 5: Physical parameters spectral evolution at a selected point of the sample.

Results of Fig. (5) extended over the studied region can be seen in Fig. (6) where 5 selected frames of the video of the physical parameters are shown.

The 4-PEM used in this work, works in transmittance, and the lack of transmittance is read as absorption, but this does not mean that the sample is absorbing the incoming photons (note that all the materials used in the multilayers are transparent in the analysed spectral range). This entails the high reflectance of the sample in the range of 500-578 nm being appreciated in the evolution of LD.

In the spectral mapping evolution of LD magnitude (Fig. (6)) a displacement of a concentric circle of low LD towards the centre of the sample is obtained. This behaviour is due to the displacement of the transmittance peak observed in Figure 3. For concentric circles on the sample, the layers' thickness remains constant and decreases as the radius of these circles increases.

A similar response is appreciated in the evolution of LB magnitude, now instead of a low magnitude circumference a high LB ring progresses towards the centre. Around the peak wavelength LB magnitude presents a maximum while LD magnitude present a minimum (Fig. (5C)), these explains the complementarity of the obtained results

With respect to the orientations of both parameters, the results obtained can be correlated with the average orientation of the nanocolums. In particular LB orientation remains constant for the studied spectrum as pointed in Fig.(5D), so it can be clearly appreciated that along a centred circumference the orientation resorts 360 degrees, as expected from the production process. Regarding LD orientation, a change in the sign of LD and LD' occurs in the resonance (Fig. (5A)). As a result of this switch, a relative rotation of 90 degrees between the two regions separated by the low LD magnitude ring is appreciated.

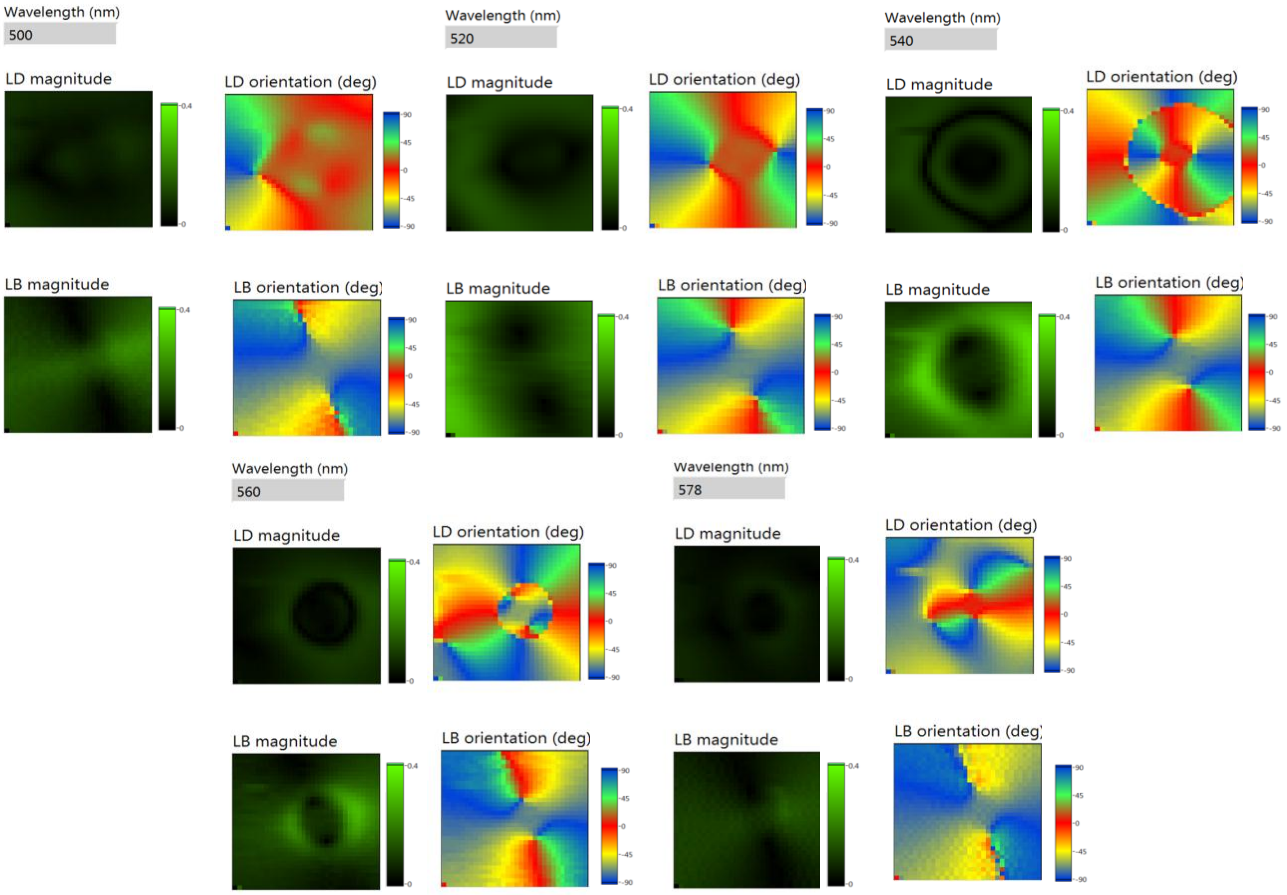

FIG. 6: Spectral evolution of the physical parameters of a Bragg micro-cavity on a glass substrate for five selected wavelengths.

V. CONCLUSIONS

- A method to determine the Mueller matrix with good spectral and spatial resolution has been implemented in the laboratory.
- The process has been fully automatized: after the instrument is configured no human intervention to obtain the spectral mapping is required.
- The anisotropic properties of Bragg Micro-cavities have been studied thanks to the aforementioned application.

Acknowledgments

I would like to thank Oriol Arteaga for giving me the opportunity to take part in this project as well as for the help provided in the last months. I would also like to thank ICMS for the collaboration and for introducing myself to innovative nanofabrication techniques with plenty of application opportunities.

[1] O. Arteaga, J. Freudenthal, B. Wang and B. Kahr, "Mueller matrix polarimetry with four photoelastic modulators: theory and calibration", Applied Optics 51, 6805- 6817 (2012).

[2] O. Arteaga, M. Baldrís, J. Antó, A. Canillas, E. Pascual, E. Bertran "A Mueller matrix microscope with a dual continuous rotating compensator setup and digital demodulation", Applied Optics 53, 2236- 2245 (2014).

[3] M. Oliva "Optofluidic thin-film sensors prepared by Oblique Angle Deposition", Ph.D. thesis, Instituto de Ciencia de Materiales de Sevilla, Universidad de Sevilla (2016).

[4] O. Arteaga, "Mueller matrix polarimetry of anisotropic chiral media", Ph.D. thesis, University of Barcelona (2010).

[5] R.M.A. Azzam, "Stokes-vector and Mueller-matrix polarimetry", Journal of the Optical Society of America A 33, 1396-1408 (2016).